Available online at www.sciencedirect.com
SCIENCE DIRECT®
International Journal of Multiphase Flow 32 (2006) 606–622
International Journal of Multiphase Flow
www.elsevier.com/locate/ijmulflow

An experimental investigation of the motion of single bubbles under a slightly inclined surface

A. Perron, L.I. Kiss *, S. Poncsák

Département des Sciences Appliquées, Université du Québec à Chicoutimi, 555 Boulevard de l'Université, Chicoutimi, Qué., Canada G7H 2B1

Received 20 December 2005; received in revised form 12 February 2006

Abstract

The movement of single air bubbles under a downward facing inclined solid surface has been investigated in motionless distilled water body. The effects of surface inclination θ and bubble volume V on the terminal Froude number are studied in details. The bubble volume was varied in the 0.3–9 cm^3 range and the inclination angles up to 10° in a gravity driven system. For a typical correlation curve of the terminal velocity u_T versus the volume at a given inclination it was found that the increase of u_T with V is not monotonous and that four distinct sub-regimes, each characterized by a specific bubble shape, exist. The effect of inclination on u_T is more sensitive at both low V and low θ. The different sub-regimes are explained qualitatively. In addition, the drag coefficients for moving bubble underneath a solid surface are presented.

Keywords: Bubble shape; Downward facing surface; Terminal velocity; Surface inclination; Drag coefficient

1. Introduction

Bubbles play a central role in many phenomena and have a fundamental importance in multiphase flow. For instance, bubbles are present in boiling, cavitation and electrolysis. In boiling as well as in electrolysis, the bubbles are usually generated on vertical or on upward facing surfaces. In some particular processes such as in nuclear engineering or during the production of aluminium, the bubbles are nucleated on downward facing surfaces. For example, Cheung and Haddad (1997) developed a hydrodynamic heat flux model to predict the critical heat flux for a saturated pool boiling on a downward facing curved heating surface. In the production of aluminium, the bubbles are generated under the carbon anode. Bubbles contribute to induce flow in the cell by transferring their momentum to the liquid via the drag force. This flow homogenises the temperature gradient underneath the anodes and distributes the reactant (alumina) to the reaction sites. Because the gas bubbles are electrically non-conducting, they constrain the current passage through the electrolysis cell. This results in an increase of the energy consumption of the process. To improve the

* Corresponding author. Tel.: +1 418 545 5011; fax: +1 418 545 5012.
E-mail address: lkiss@uqac.ca (L.I. Kiss).

0301-9322/$ - see front matter © 2006 Elsevier Ltd. All rights reserved.
doi:10.1016/j.ijmultiphaseflow.2006.02.001

understanding of the bubble effects on the transport phenomena in the cell, the mechanism and the intensity of the momentum transfer must be known. It is well known that the behaviour of the bubble layer underneath the anode varies markedly with a little deviation of the surface inclination from the horizontal. In an electrolysis cell there are two kinds of moving bubbles: vertical and quasi-horizontal bubbles. The former case has been studied extensively both experimentally and theoretically while only a few papers have been devoted to the second case. The purpose of our study is to determine the effect of inclination and bubble volume on the terminal velocity of a bubble moving underneath a surface. The values of the drag coefficient presented in this work for a bubble moving underneath a slightly inclined plate are essential in order to develop a mathematical model to obtain a realistic flow pattern within the electrolyte region. Before presenting our results, we discuss the vertical rise of a bubble in an infinite medium and bubble rising at inclination in a finite medium.

It is well known that for an air bubble rising vertically in water, there are three regimes where different mechanisms control the terminal velocity of a bubble. The equivalent diameter d, generally defined as

$$d = \left(\frac{6V}{\pi}\right)^{1/3} \tag{1}$$

based on the bubble volume V, may be used to separate the different regimes. The first region is characterized by $d < 0.07$ cm. In this zone, the bubbles behave as rigid spheres and the terminal velocity u_T is controlled by the viscous drag. The bubble path is rectilinear. At ($0.07\text{ cm} < d < 0.14$ cm) the viscous shear stress is reduced by the circulation of gas inside the bubble and the u_T is increased in a pure system. The reader is referred to Tomiyama et al. (1998) for a recent review. The second region controlled by the surface tension force ($0.14\text{ cm} < d < 0.6$ cm) is the most complicated. Many authors studied this regime like Peebles and Garber (1953); Saffman (1956); Hartunian and Sears (1957); Mendelson (1967), Ellingsen and Risso (2001) and Tomiyama et al. (2002). The formation of vortices in the wake of the bubble increases the drag and the bubbles are not anymore spherical but rather oblate spheroids. This region is characterized by bubble motion such as zigzag and helical as well as by a widely scattering u_T. Several authors have attributed the discrepancy in the measured u_T to a difference in surfactant concentration between the nose and the rear part of the bubble. Recently, Ellingsen and Risso (2001) showed that for a bubble diameter of 2.5 mm, the effect of the surfactants is negligible. Tomiyama et al. (2002) showed experimentally and theoretically that the scattering in u_T might be caused by differences in the bubble release conditions. They developed an expression for u_T in the surface tension dominated regime, based on the momentum jump condition at the interface of the bubble and using the potential flow theory. The expression is a function of the bubble diameter, fluid properties and bubble shape. The third regime occurs when $d > 0.6$ cm. The bubble volume is large enough to form a spherical cap. The terminal velocity is controlled by the inertial force, i.e. by the form drag. Davies and Taylor (1950), considering zero surface tension and an inviscid liquid, obtained an expression for u_T in both pure and contaminated liquids:

$$u_T = I\sqrt{gr_c} \tag{2}$$

where g is the gravitational acceleration, $I = 0.67$ is a constant and r_c is the radius of curvature at the bubble nose. Haberman and Morton (1953) found a more useful form of Eq. (2) in terms of the equivalent diameter d:

$$u_T = J\sqrt{gd} \tag{3}$$

where $J = 0.72$.

Several experimental and theoretical works have also been published on the bubble motion in a finite stagnant medium. Bertherton (1961) and Goldsmith and Mason (1962) studied the motion of long bubbles in closed vertical tubes. A long bubble in a tube is defined as a bubble with a terminal velocity and a nose curvature independent of its length, for lengths greater than a few tube radii. The two papers showed that when the surrounding liquid wets the wall, there is a liquid film between the wall and the moving bubble. Goldsmith and Mason (1962) measured the velocity profile in the liquid film and the result was in very good agreement with their theoretical prediction. Zukoski (1966) studied experimentally the influence of inclination on the motion of long bubbles in closed tubes. He noted that the propagation of a long bubble was complex because the bubble geometry changes with inclination. In general, the experiments showed that the u_T increases to a

maximum value as the inclination angle decreases from the vertical to 45°. Further decrease of the inclination angle 45° to the horizontal position results in a decreasing rate of propagation. Spedding and Nguyen (1978) also investigated the bubble rise in inclined tubes. They showed that the Froude number Fr_1 for the steady motion, defined as

$$Fr_1 = \frac{u_T}{\sqrt{gD_T}} \tag{4}$$

where D_T is the tube diameter, increases markedly with the bubble volume at low tube inclinations close to the horizontal orientation. Beyond 2° of inclination, the Fr_1 becomes nearly independent of the bubble size. They mentioned that at low angles, the bubble volume had to be greater than 20 ml before bubble movement occurred. For the effect of the inclination on the propagation rate for a given bubble size, they observed the same tendency as Zukoski (1966).

The number of articles published about the motion of bubble under an inclined surface is small compared to the number of works dedicated to the study of bubble rising through an unbounded medium. Maxworthy (1991) studied the motion of large bubbles moving under an inclined plate for bubble volumes ranging from 5 cm^3 to 60 cm^3 at intervals of 5 cm^3. The working liquid was water. The surface inclination was varied between 5° and 90° from the horizontal. The slope was increased at intervals of 5° except for the values of 55°, 65° and 75°. It was found that the terminal velocity of a bubble increases monotonously with the bubble volume and the rise velocity reaches a maximal value at an inclination of about 50°. In all experiments, the bubble motion was controlled principally by the inertia. Chen et al. (1992) experimentally studied the role of surface inclination, bubble volume and channel width on the terminal velocity of large bubbles moving under a surface. The bubbles were produced by injecting a known volume of air into a downward facing cup with a syringe. The cup was inversed to release the bubble. They studied the effect of inclination up to 12°, the bubble volumes ranging from 1 cm^3 to 40 cm^3 while the widths used were 100 mm, 55 mm, 25 mm and 16 mm. It was found that the terminal velocity increased monotonously with the bubble volume. Only seven points (V, u_T) were used to characterize the whole range of volume from 1 cm^3 to 40 cm^3 for a given inclination. Masliyah et al. (1994) studied the rise velocity of small bubbles of air along an inclined surface in water–glycerol solutions. The bubble volume covered a range from 0.0026 cm^3 to 0.013 cm^3 and the inclination varied between 35° and 90° from the horizontal. It was found that the bubble terminal velocity increases monotonously as the inclination angle increases toward the vertical. They did not find a critical inclination angle at which the velocity is maximal. Perron et al. (2005) investigated the movement of single large bubbles under an inclined surface. When a bubble is initially attached to a surface with a pinned triple line (meaning the presence of a dry spot), it was found that there might exist two markedly different regimes of movement if the buoyancy force overcomes the retarding surface tension forces. In general, there is a creeping motion followed by the movement of the bubble on a wetting film separating it from the solid plate. The formation of a wetting film is caused by a perturbation of the equilibrium state such as the pinning of the triple line caused by a chemical impurity or a surface default at the bubble nose. This results in a deformation of the bubble and a decrease in the magnitude of the surface tension force. The minimal velocity which allows the existence of the liquid film is reached and the bubble begins to glide on it. It was observed that u_T of a creeping bubble was about one order of magnitude smaller than that of a bubble moving on the wetting film. The distance travelled by a creeping bubble is inversely proportional to the bubble volume at a given inclination. If the bubble volume exceeds a certain value, the bubble travels almost along the whole plate on the wetting film.

In the series of experiments presented here, the influence of surface inclination and bubble volume on the terminal velocity of relatively large bubbles rising on the wetting film regime is studied.

2. Experiment

A schematic diagram of the experimental setup is shown in Fig. 1. The length, width and depth of the plexiglas tank were 1.20 m, 0.34 m and 0.34 m, respectively. The solid surface under which the bubble moved was represented by a plexiglas plate 1 cm thick, 16 cm wide and 90 cm long fixed on the tank sides by two pivots. To avoid deformation (curvature) of the plate caused by gravity effects, two reinforcing metal rods were fixed

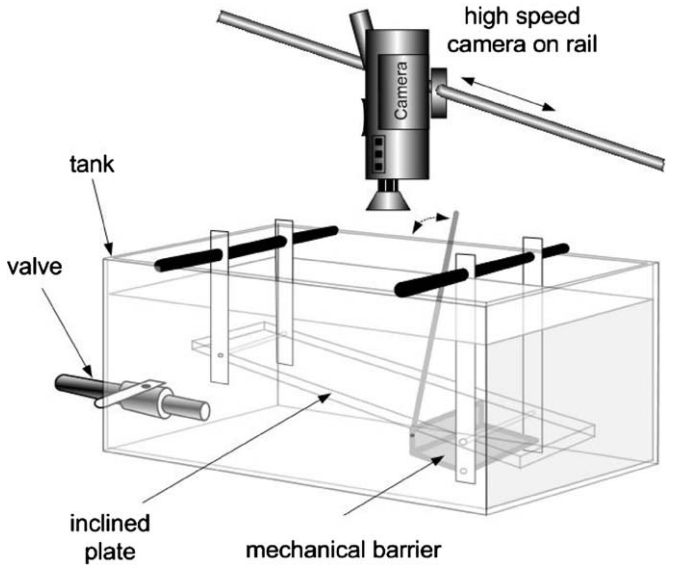

Fig. 1. Schema of the experimental apparatus.

on both sides. The frame allowed an inclination up to 10°. At 1° of inclination, the bubble could not reach the appropriate velocity to maintain the wetting film over the whole length of the plate. For this reason, the experiments were carried out in the 2–10° range. The inclination angle was measured with a digital inclinometer with a display resolution of 0.01° for angles below 10°. At each angle, five readings were taken at three different positions to verify the flatness of the plate. The working liquid was distilled water. The air bubbles were produced by two different methods. In the first, the bubbles were created directly under the surface, behind a movable barrier using a precision syringe. The dry spots were spontaneously created within 1 s. The bubbles were then released by moving the mechanical barrier very slowly to avoid the acceleration of the fluid around the bubble. This method was useful to study the whole range of bubble sizes only at high inclination angles. At low inclination angles, for small bubbles, there was no transition from the creeping motion to the ''bubble on the wetting film'' regime. Therefore, to study the smaller bubbles at low inclination, we used the ''inversed cup'' technique developed by Chen et al. (1992) and described above. Several tests were carried out to verify whether these two methods of bubble production could influence the terminal velocity of a bubble. It was found that the terminal velocity was always the same independently of the way the bubbles were created. With both techniques, the bubble volumes were varied in the 0.3–9 cm^3 range for each inclination. A sufficient time elapsed between the experimental runs to ensure that the liquid was at rest. The effect of the reduction in hydrostatic pressure was negligible in the studied range of inclination angles. During the experiments, the temperature of water body was kept constant at 20 °C.

To obtain the trajectory of the bubble $x(t)$, the instantaneous velocity $u(t)$, the shape, the instantaneous aspect ratio $r(t)$ (in the plane of the surface), the time-averaged aspect ratio r and the terminal velocity u_T, a track-mounted high-speed digital camera was used to follow the moving bubble. Identification of the major b and the minor a axes is presented in Fig. 2. The axis a is parallel to the direction of the bubble movement while the axis b is perpendicular to it. For the recording, the PCI 2000 hi-speed camera was set to a resolution of 476×256 pixels and a shutter speed of 1/2000 s. The recording rate of 125 frames/s permitted to capture the whole movement of the bubble under the plate. A transparent grid (5 mm/division) was placed over the plate in order to identify the position of the bubble as a function of time. The position of the bubble was obtained by identifying the center of the bubble in the plane of the solid surface. The instantaneous velocity in the x direction and the instantaneous aspect ratio were calculated by using the formulae

$$u(t) = \frac{x(t+\Delta t) - x(t)}{\Delta t} \tag{5}$$

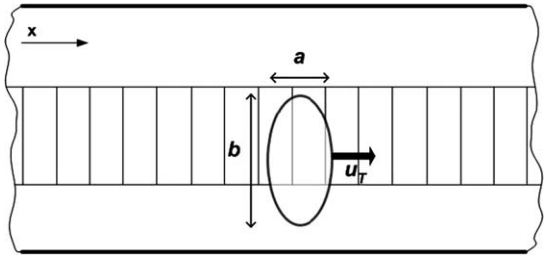

Fig. 2. Identification of the axes of a bubble.

$$r(t) = \frac{b(t)}{a(t)} \tag{6}$$

where the time step $\Delta t = 0.12$ s corresponds to 15 frames. This value of Δt seems to be large in comparison with other works (Tomiyama et al., 2002), but it is important to mention that in this work we analysed the average values and not the oscillations of these quantities. The calculation of the instantaneous velocity indicated when the terminal velocity was reached. It is clear that the identification and the interpretation of $u(t)$ are more difficult for a deformable bubble than for a rigid one. Moreover, the distinction between shape and path oscillations becomes less evident. The terminal velocity was calculated from (5) with a longer known distance and a larger known time interval in order to decrease the uncertainties linked with this measurement. Each experiment was repeated three times. The averaged results are presented in this work. The difference between the values of bubble terminal velocity for the same experiment was generally small, about 3%. For the whole series of experiments done in the frame of this work, the maximum difference was 7%.

Position, instantaneous velocity and instantaneous aspect ratio values for two different bubble volumes (0.3 (a) and 2 cm^3 (b)) as function of time are presented in Fig. 3 for an inclination of 6°. The smaller bubble was produced with the inverted cup technique while the other one was released using the mechanical barrier. The bubble (a) on the left had a nearly non-deformed shape. After 1 s the terminal velocity was reached. The amplitude of the fluctuations of both the aspect ratio and velocity were weak. On the right side, the bigger bubble (b) was deformable. Although the amplitude of the fluctuations was non-negligible, the terminal velocity was also reached in less than 1 s. To assure that the terminal velocity was reached in any experiment, the first point used to compute it was always taken after 1.5 s from the onset of the wetting regime after the transition.

3. Results and discussion

3.1. Effects of bubble volume and inclination angle on the bubble shape

The shape of a bubble initially attached to a surface depends strongly on its relative position. For instance, there is a marked difference in the shape of bubbles below or above a horizontal solid surface. For the former, the gravitational force presses the bubble against the upper wall whereas for the latter, the gravity tends to break away the bubble from the surface. Bubble under a solid surface will move either if there is an inclination or under the effect of a liquid flow while for a bubble on an upward facing surface, the buoyancy is free to act to detach the bubble. Fig. 4a shows the shape of a static bubble with different volumes. The radius of the contact surface, the height of the bubble and the contact angle are all shown in the vertical section. For small volumes the bubbles are spherical and they become gradually flattened as the volume increases. For a system of air–water–plexiglas the static contact angle θ_c is about 80° (Pruppacher and Klett, 1978). In the plane of the solid surface, the contact zone of the bubble appears as a perfect circle with a radius of R_c. The height (depth) of a bubble increases with increasing bubble volumes until it reaches a maximal value h_{max}. A further increase of the volume decreases slightly the height of the bubble until a limiting value h_{lim} as shown in Fig. 4b. The points presented here are for an air bubble hooked under a plexiglas plate. The upper limit h_{max}, for the static case is given by Hartland and Hartley (1976):

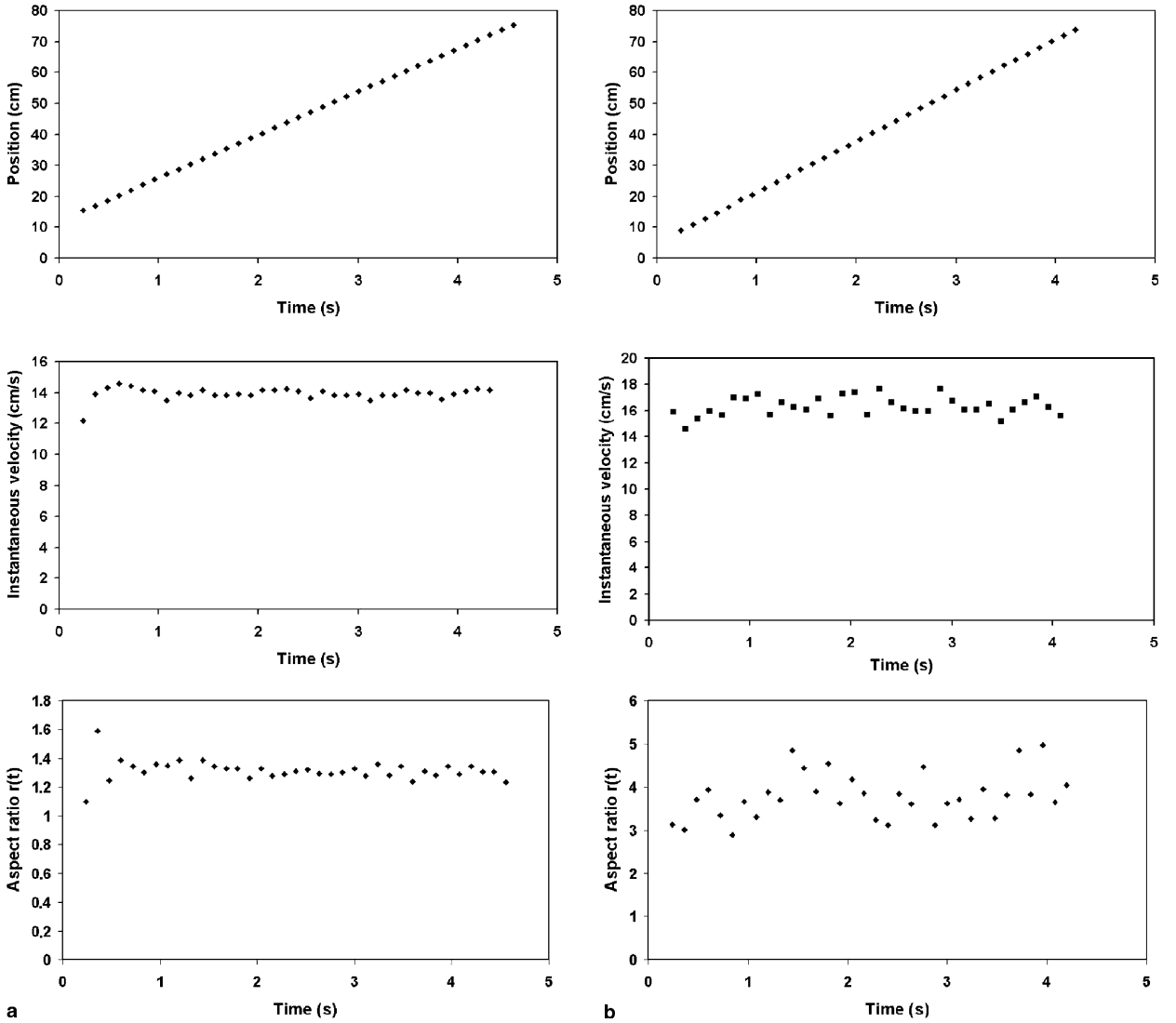

Fig. 3. Position, instantaneous velocity and instantaneous aspect ratio of different bubble volumes as function of time at an inclination of 6°: (a) 0.3 cm^3, (b) 2 cm^3.

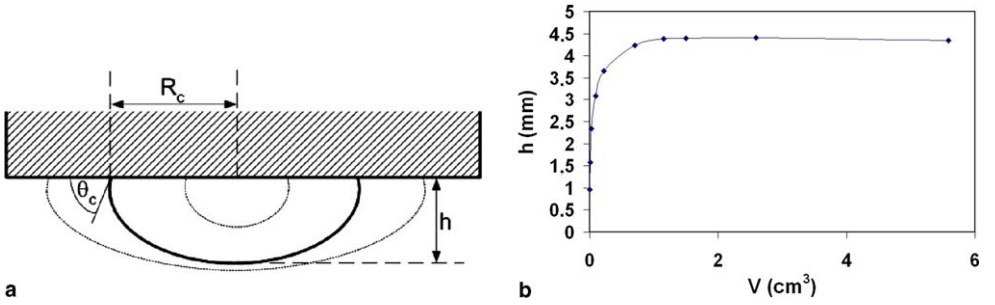

Fig. 4. (a) Shapes of bubbles of different volumes under a surface. (b) Height (depth) of bubbles as function of volume for a static bubble.

$$h_{\max} = \left(-0.190(\pi - \theta_c)^2 + 1.293(\pi - \theta_c) - 0.053\right)\left[\frac{\sigma}{(\rho_L - \rho_G)g}\right]^{1/2} \tag{7}$$

where σ is the liquid surface tension, θ_c is expressed in radians and ρ_L and ρ_G are the liquid and gas densities, respectively. For the air–water–plexiglas system at 20 °C, the maximal height is 4.44 mm while the limiting depth as given by the same reference

$$h_{\lim} = \left[2(1 - \cos(\pi - \theta_c))\frac{\sigma}{(\rho_L - \rho_G)g}\right]^{1/2} \tag{8}$$

equals 4.18 mm.

Bubbles moving under a solid surface generally have a complex three-dimensional shape. Fortin et al. (1984), Solheim and Thonstad (1986) and Zoric and Solheim (2000) observed, that the front part of large, fast moving bubbles is thicker than their rear part. The two regions with different thicknesses are separated by a step-wise level variation of the lower gas–liquid interface – a phenomenon known as hydraulic jump in the case of free surface flows. Haupin (1971) measured the voltage gradient in the interpolar space in an industrial reduction cell. He found that occasionally, there were contacts between the probe and gas bubbles as far as 2 cm from the anode surface while the maximal height is about 4.3 mm for the CO_2–cryolite–carbon system in static condition for steady state operation. Kiss et al. (2004) observed a periodic "rolling motion" of the interface. Furthermore, the hydrogen bubble tracer method permitted to note that this periodic motion of the interface might be connected with vortex formation (Perron et al., 2005). Consequently, the shape of a moving bubble in the plane of the solid surface is not a circle anymore. In this paper, the bubble shape in this plane is described.

The tendency of the aspect ratio as a function of the bubble volume is shown in Fig. 5 for a given inclination. The characteristic shapes C, D, E and F are shown in Fig. 8. The limits of a class depend upon the surface inclination angle. Furthermore, as the inclination angle increases, the curve presented in Fig. 5 is translated horizontally to the left. At high inclinations, certain sub-regimes such as A, B, C and D can either disappear or shrink in width, while at low inclination, the zones E and F might even not exist. The transition between the sub-regimes is not drastic except for the transition between B and C.

In zone A the bubble is immobile. As it was mentioned earlier, when a bubble is attached under a horizontal surface, the contact angle, measured through the liquid phase, equals the equilibrium value θ_c. The integral of the surface tension force along the triple line vanishes. When an attached bubble is immobile under an inclined surface, the contact angles along the triple line differ from the equilibrium values. The upper contact angle is smaller and the lower contact angle is larger than the equilibrium value. In that case, the contact angle is receding at the front part of the bubble while it is advancing at the rear part. Therefore, the in-plane component of the buoyancy force is balanced by the difference in the contact angles. In other words, the integral of the surface tension along the contact line equals the component of the buoyancy force. Until that the advancing and receding angles reach their critical values, θ_a and θ_r ($\theta_a > \theta_c$, $\theta_r < \theta_c$), respectively, the bubble is immo-

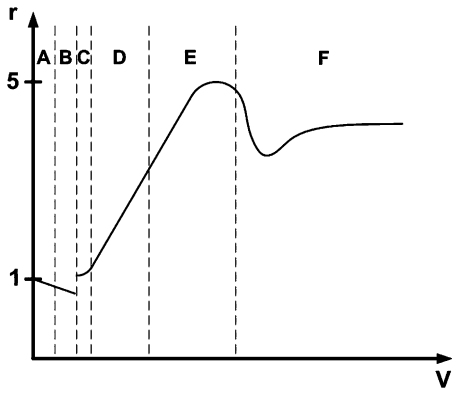

Fig. 5. Tendency of variation of the aspect ratio as function of the bubble volume at a given inclination.

bile. The difference in the angles ($\theta_a - \theta_c$) is the hysteresis reflecting the surface inhomogeneities of the plexiglas. In other words, if the surface was homogeneous and perfectly smooth, the sub-regime *A* would not exist. As the bubble volume increases, the value of the receding angle approaches θ_r and the advancing angle θ_a. The gravity force deforms the bubble more and more until the difference ($\theta_a - \theta_c$) cannot balance the buoyancy anymore. At this moment, the bubble starts to move slowly. The sub-regime B is characterized by a slow, strongly attenuated movement. There is a competition between the dynamic wetting and dewetting of the surface. This phenomenon is related to the movement of the triple line. A nearly constant velocity was observed in this sub-regime. Some perturbations could happen but the system returns to its steady equilibrium state. In this sub-regime the shape of the contact line is oval and the longer axis lies in the direction of the displacement.

As the bubble volume is increased (at the same inclination), there is an interesting transition from the creeping movement regime to the bubble gliding on the wetting film regime. Although the aim of this work is the study of the bubble movement in the wetting regime, it can be interesting to describe the complete transition as function of time. Fig. 6 below shows the instantaneous velocity of the front and the rear parts of a bubble as function of time; before, during and after the transition. The penetration of the wetting film at the bubble nose can also be observed in Fig. 6b and c. The bubble volume is 2.3 cm^3 and the inclination angle is 4°. The images are captured by using the same experimental setup presented in Fig. 1 but with a recording rate of 250 frames/s. Before 2.5 s, the creeping bubble has a nearly constant velocity, about 2–3 cm/s (Fig. 6a). The longer axis of the bubble lies parallel to the direction of the movement. At about 3 s, the bubble nose encounters microscopic obstacles. The pinning retards the dewetting causing a diminution of the receding angle at the front part. The penetration of the aqueous layer starts since the advancing part rolls over the receding part (Fig. 6b). At this time, the bubble nose and the rear part of the bubble do not experience the same forces. Indeed, the nose is not exposed to the retarding surface tension force. The front part is freer to move, causing an elongation of the *a* axis of the bubble in the direction of the movement as shown in Fig. 7. The gravity force works against the retaining forces present at the rear but also against the surface tension of the bubble by deforming it. When the penetration is finally completed, at about 3.5 s (just after the instant shown in Fig. 6c), the rear part is accelerated to a high velocity of about 40 cm/s. This dynamic effect transforms the elongated shape almost instantaneously into a near circular one. The length in the movement direction changes from 3.5 cm before the transition to 1.5 cm after it. The transition being completed (Fig. 6d), the bubble glides on the wetting film with a velocity of about 14 cm/s. As shown in Figs. 6 and 7, the transition is drastic and evident in terms of bubble shape as well as in bubble velocity. Its duration is about 1 s. At high inclinations and/or at high bubble volumes in a gravity driven system, the distance travelled by a bubble in the creeping regime becomes negligible since the tendency of the rollover described previously is greater the larger the bubble volume and/or the inclination of the surface. In an electrolysis cell, where a liquid flow exists, the

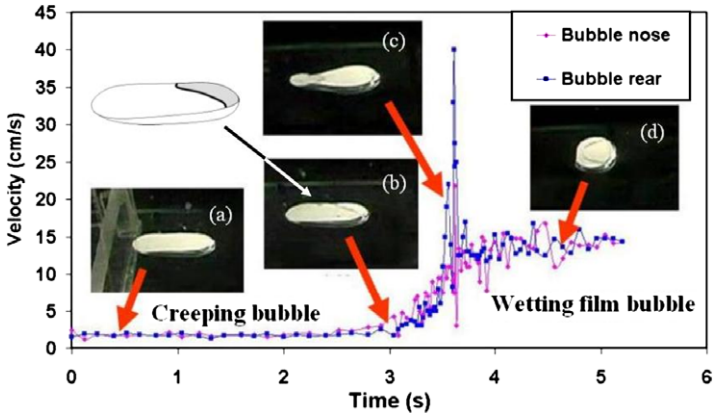

Fig. 6. Instantaneous velocity of the nose and the rear parts of a bubble of 2.3 cm^3 before, during and after the transition at an inclination of 4°. (a) Creeping bubble regime, (b) the penetration of the liquid film begins, (c) maximal elongation of the bubble in the direction of the movement, and (d) wetting regime. All the four bubbles move toward the right.

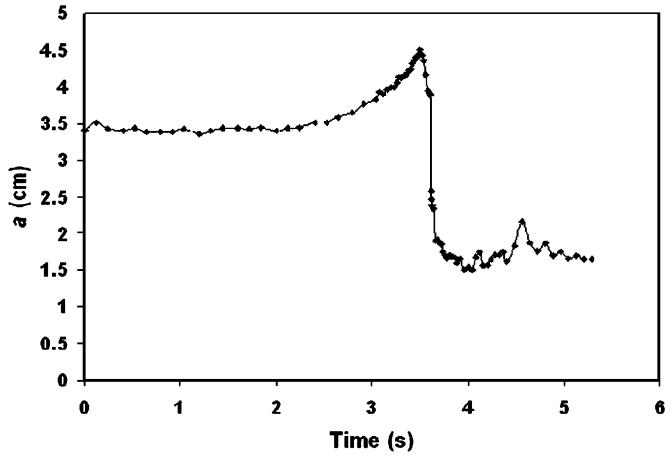

Fig. 7. Evolution of the axe a of a bubble during the transition for a volume of 2.3 cm^3 and at an inclination of 4°.

bubble is accelerated not only by the buoyancy but also by the drag force. Then, the creeping regime is even more negligible. This is the reason why the present work emphasizes on the wetting regime described below.

For a bubble moving on the wetting film, four different characteristic shapes have been observed in the present work. As the bubble volume and the terminal velocity increase from the values that correspond to the shape C to the values marking the shape F, the role of the inertia controlling the terminal velocity becomes more and more important for larger bubbles. The influence of the viscous force decreases from C to F. The role of the surface tension is more difficult to evaluate because it has an indirect effect on the bubble velocity. The surface forces tend to reduce the deformations caused by the flow that is induced by the movement of the bubble itself. However, for large bubbles it is clear that the role of the surface tension force becomes less important and the bubble shape is rather controlled by dynamic effects.

The bubble shape in the sub-regime C in Fig. 8 is nearly circular. The radius of curvature at the bubble nose in the plane of the solid surface is slightly larger than the one at the bubble rear. The amplitude of the fluctuations of the aspect ratio is weak as it shown in Fig. 3a. The mean value of the aspect ratio r is about 1.3. The path is almost rectilinear. Sometimes a very small path oscillation was found near the end of the travel. In the transversal plane, the interface contour behaved as if it were solid. The bubble shape C is called *semi-rigid bubbles*. As the volume increases, the bubble shape D is obtained. The elongation in the direction perpendicular to the movement becomes more significant. The shape oscillations are periodic and more pronounced than in the case of the previous class. Therefore, the radii of curvature at the front and the rear part vary periodically within a certain range. The curvature is positive at the front of the bubble whereas it can be either zero or slightly negative (concave) at the bubble rear. The path of the bubble is rectilinear. The bubble D is called "*oval oscillating bubble*". Its aspect ratio may reach a value around 2.5. The formation of a hydraulic jump has

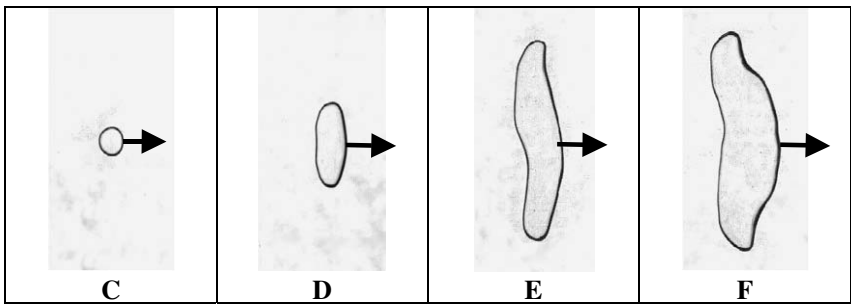

Fig. 8. Characteristic shapes of "bubbles on the wetting film" under an inclined surface at a given inclination. The volume increases from C to F. All the four bubbles move toward the right.

been observed in the vertical cross section at the end of this sub-regime. A further increase in volume gives the bubble shape E. These long, tubular bubbles could be easily deformed in all directions. However, the longer axis (b) is always perpendicular to the bubble motion. The curvature at the front and the rear part could be either positive or negative. As it is shown in Fig. 3b, the amplitude of oscillations in $u(t)$ and $r(t)$ are important. The instantaneous aspect ratio reaches a value of about 5. It is difficult to distinguish shape and path oscillations, but in general the bubble trajectory was nearly rectilinear. A hydraulic jump was always observable in the vertical cross section. Deformations may be created by the generation and release of non-symmetric three-dimensional trailing-vortices. The bubble E is termed *deformable bubble*. The last class of observed bubble shapes is particular. Even if there are important deformations, the bubble has a general characteristic: a bulge with a positive curvature is always present around the leading edge. This is rather a dynamic effect than the result of the action of surface tension forces as at this bubble size the impact of the latter is weak. At the rear part, the curvature could be either negative or nearly zero. Similarly as for the bubbles E, a hydraulic jump was always seen in the vertical section. The aspect ratio increases slightly up to a limiting value nearly constant at high bubble volumes. Two "tails" can be observed at the lateral ends of the bubble. The bubble ends are thinner than the center of the bubble. The radius of curvature changes sign along the leading edge as seen from above. Although the amplitude of the fluctuation of the aspect ratio is smaller than that was in the case of the *deformable bubbles*, the shape oscillations remain important. The bubble path was near to rectilinear. The bubble F is called "*bulged bubble*". The tail formation is likely provoked by the generation and release of a pair of symmetrical trailing-vortices. The effects shaping these bubbles require a deeper analysis of the bubble–liquid interaction. The mechanical relation between the bubble deformation and the distribution of vorticity is very difficult to establish and it is beyond the scope of the present work.

To resume, the wetting film bubble regime may be divided into four subclasses as the volume increases: *semi-rigid bubble*, *oval oscillating bubble*, *deformable bubble* and *bulged bubble*. Viscous and surface tension forces may play a role for small bubbles while for larger bubbles, the inertia controls principally the movement. It will be seen later that the bubbles of the fourth class (bulged bubbles) are characterized by a nearly constant drag coefficient.

3.2. Effect of bubble volume on the terminal velocity

It is well known for a vertical rising bubble that when the terminal velocity is reached, the two forces acting on it are the buoyancy and the drag forces. These forces are of equal magnitude but their directions are opposed. For a bubble moving under an inclined surface, it is the component parallel to the surface of the buoyancy force which acts against the drag force. Fig. 9 shows raw data of the terminal velocity u_T as function of the equivalent diameter d for inclination angles of 2°, 4° and 10°. The rate of increase of u_T with the volume

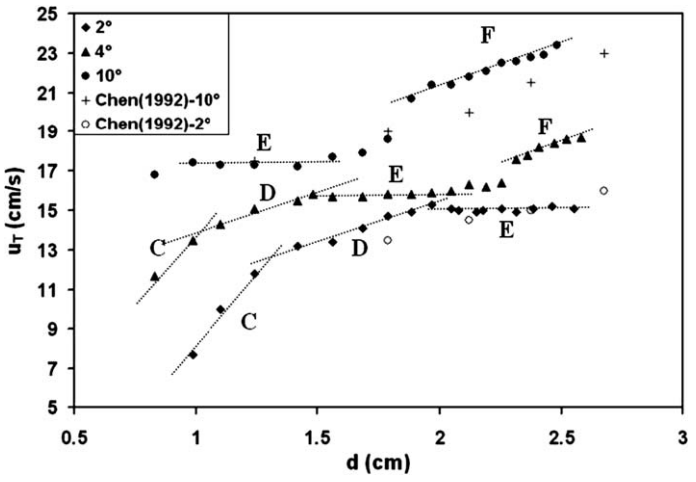

Fig. 9. Raw data of the terminal velocity as function of the equivalent diameter.

is not monotonous for all inclination angles. The curve at 4° can be divided into four nearly linear regions. Correlating the sections of the graph with the corresponding observed bubble shapes, it is found that each zone is characterized by one of the bubble shapes presented in the previous section. This observation shows also that the way that u_T increases when the volume is increased depends on the bubble shape. At 10° the zones C and D do not appear. Below an equivalent diameter of 0.87 cm, it is not certain that these zones appear at 10° because a minimal velocity is required to maintain the wetting film between the bubble and the plate. On the other end of the parameter range, one may expect that the bulged bubble region F exists beyond the equivalent diameter of 2.58, the last point measured in our experiments. At low angles, it is the *semi-rigid bubble* region C where u_T increases the most markedly with the bubble volume. In the zones D and F the curves have nearly the same slope, smaller than in the *semi-rigid bubble* region. The *deformable bubble* region is interesting. As the bubble volume increases, the terminal velocity remains almost constant and the aspect ratio reaches a maximal value. We can imagine the long bubble as a cylinder with its longer axis perpendicular to the movement so the flow around it is characterized by its diameter. It seems that for a given inclination, the diameter reaches a maximal value and a further growth results solely in an elongation in the direction perpendicular to the motion. Moreover, the bubble is long enough that the trailing-vortices at the ends do not represent an important influence. The bubble might be considered like an infinite cylinder. Hence, the terminal velocity would be constant with the bubble volume for this bubble shape. Results obtained by Chen et al. (1992) are shown on the graph for inclinations of 2° and 10°. Their experiments were carried out in a channel with a width of 100 mm. Generally their values of the terminal velocity are slightly lower and the behaviour of the curve is more linear than our results.

The influence of inclination on the terminal velocity is shown in Fig. 10. In the studied range, the terminal velocity increases always as the inclination angle increases for a given bubble volume. For small bubbles, the increment is higher at low than at high inclinations whereas for large bubbles, the increase is nearly linear. For instance, for a given bubble size of $d = 0.985$ cm, the effect of changing θ from 2° to 6° is to double the value of u_T at 2°. As pointed out by Zukoski (1966) the influence of the inclination angle on the terminal velocity is rather complex. First, the angle influences the magnitude of the component of the buoyancy force and consequently, it deforms the shape of the moving bubble.

We shall discuss briefly the dimensionless parameters used in this section before presenting the experimental results in a dimensionless form. The problem of the rising of an air bubble of equivalent diameter d with a terminal velocity u_T under a tilted plate has similarities with a bubble rising vertically through a motionless liquid under the same gravitational acceleration g. The properties of the working liquid that influence the bubble motion are the density (ρ_L), the kinematic viscosity (υ_L) and the surface tension (σ). The corresponding values for the density and viscosity of the air in the bubble are very small compared to those of the liquid and therefore they are negligible. By considering three physical dimensions such as mass, length and time

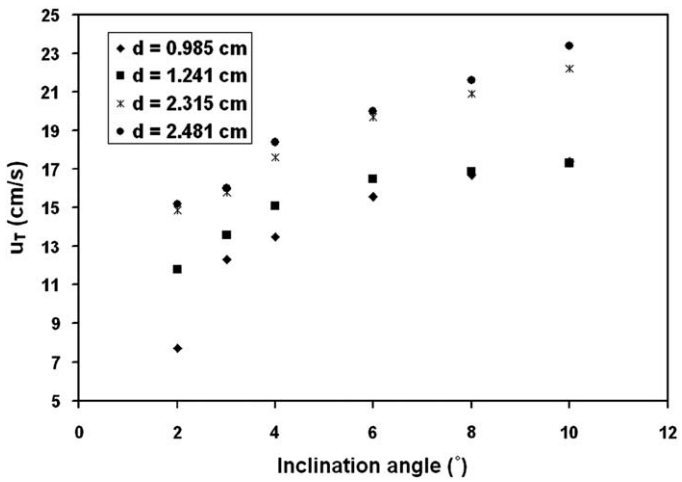

Fig. 10. u_T as function of θ for different d.

and using the Buckingham Π theorem, the system of variables can be reduced to three independent dimensionless groups. The terminal velocity being measured, Maxworthy et al. (1996) showed that in fact there are two independent parameters such as the Bond number and the Morton number expressed as

$$Bo = \frac{\rho_L d^2 g}{\sigma} \tag{9}$$

$$Mo = \frac{g v_L^4 \rho_L^3}{\sigma_L^3} \tag{10}$$

and one dependent parameter which is function of the u_T. The surface inclination angle θ is already a dimensionless quantity and must be added to the list of independent parameters. Therefore the system is described by three independent parameters (Bo, Mo, θ) and one dependent parameter. The Morton number is strictly related to the liquid properties. In this work, the working liquid (water) is the same for all experiments, therefore the Mo is constant and it does not play a role in our results. Material properties of water used to calculate the non-dimensional numbers as well as the value of the Morton number are presented in Table 1. As pointed out by Maxworthy (1991), the Froude number defined as

$$Fr = \frac{u_T}{\sqrt{dg \sin\theta}} \tag{11}$$

is the dependent dimensionless parameter the most appropriated from both dynamical and dimensional point of view. Fig. 11 shows the experimental results in a dimensionless form for inclination angles of 2°, 3°, 4°, 6°, 8° and 10°. All the curves beyond 3° present a sensibly constant Froude number at high Bo numbers for the studied range of bubble volumes and inclination angles. It means that the ratio of the inertial and gravity forces remains constant even if the volume is increased. The plateau corresponds to the *bulged bubble* subregime.

Table 1
Physical properties of the working liquid (water), and the values of the Morton number at a temperature of 20 °C (data taken from White, 1999)

Density ρ_L (kg/m^3)	998
Kinematic viscosity v_L (m^2/s)	1.005×10^{-6}
Surface tension σ (N/m)	0.073
Morton number Mo	2.557×10^{-11}

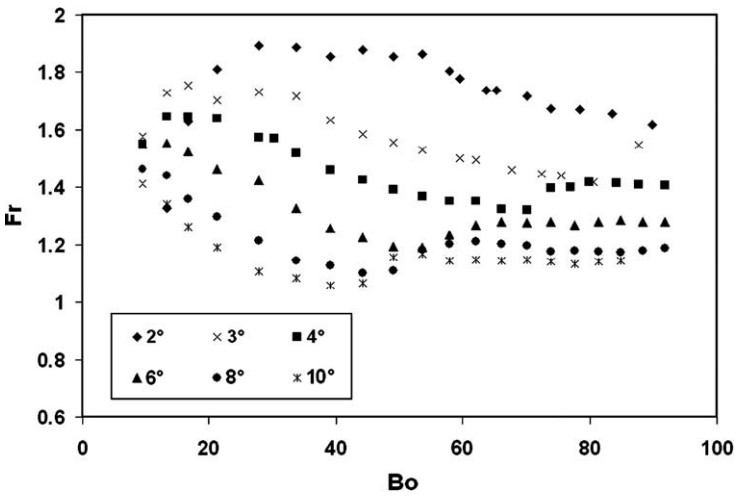

Fig. 11. Fr as function of Bo for different inclination angles.

To resume, the results show that the terminal velocity increases with the bubble volume in the studied ranges of V and θ. The increase is not monotonous.

3.3. Drag coefficient of a moving bubble underneath a surface

For the mathematical modelling of a bubble driven flow, the intensity of the momentum exchange between the two phases is required. Generally, it is achieved by adding a momentum source term in both sets of phase equations for the two-fluid models. That source term is proportional to the drag coefficient C_d and other variables. As mentioned before, the terminal velocity of a bubble moving under a solid plate is reached when the component parallel to the surface of the buoyancy force equals the drag force. Here the density of air is not neglected in order to improve the precision of the results. The component of buoyancy force is given by

$$F_B = (\rho_L - \rho_G) V g \sin\theta \tag{12}$$

The drag force model is given by (Clift et al., 1978):

$$F_d = C_d A_T \frac{\rho_L u_T^2}{2} \tag{13}$$

By equating (12) and (13), we obtain

$$C_d = \frac{2}{A_T} \frac{\Delta\rho}{\rho_L} \frac{1}{u_T^2} V g \sin\theta \tag{14}$$

where $\Delta\rho = (\rho_L - \rho_G)$ and A_T is the frontal area. For a spherical bubble, $A_T = \pi d^2/4$. The shape of a bubble moving under a solid surface is different from a sphere as we have shown it previously. To estimate the cross section area, we tried different forms such as half-circle, half-ellipse and rectangle. The comparison of the shapes of the curves was done with the classical representation of d equivalent and it was found that representing the frontal area by a circle does not give rise to a loss of physical sense. Therefore the C_d can be expressed by

$$C_d = \frac{4}{3} \frac{\Delta\rho}{\rho_L} \frac{gd}{u_T^2} \sin\theta \tag{15}$$

There are several ways to plot the drag coefficient. Maxworthy et al. (1996) proposed to express C_d as function of the Morton and the Reynolds (Re) numbers, the latter defined as

$$Re = \frac{u_T d}{\upsilon_L} \tag{16}$$

The bubble Reynolds number represents the ratio of the inertial to viscous drag force. Fig. 12 shows the variation of C_d versus Re. Regarding the two curves at the lowest and highest inclinations, there are strong resemblances between them and the well-known curves of C_d versus Re for a vertically rising bubble. At low inclination angles (2° in the graph), there is a zone where C_d decreases with increasing Re. For a rising unbounded bubble, it is well known that the viscous regime is characterized by a reduction of the drag coefficient as the Re is increased. Therefore the presence of this tendency suggests that the viscous force may play a role on the motion of small bubbles at low inclination angles. Also, the characteristic shape in this range is the *semi-rigid bubble*. The transition to the next characteristic shape is marked by the increase of the drag coefficient with Re. This tendency is present at all inclination angles. In this range, the C_d increases strongly at high inclination angles. The drag coefficient reaches a maximum and then decreases until the *bulged bubble* limit. A C_d nearly constant characterises this sub-regime, which means that the bubble movement is principally controlled by the inertia.

The drag coefficient can also be expressed as a function of the independent parameter Bo, as it is shown in Fig. 13.

In order to help the application of mathematical modelling, we determined the approximate functional forms of these curves in the *deformable* and *bulged* sub-regimes. Unfortunately, the number of points in the *semi-rigid* and *oval oscillating bubble* sub-regimes is too small to determine reliable correlations. For these

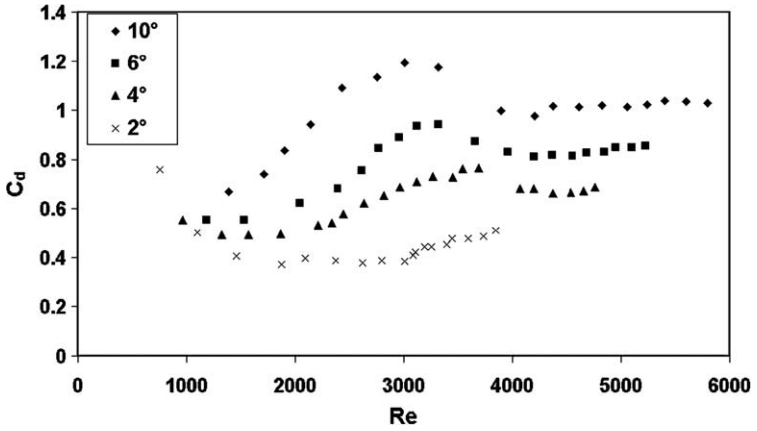

Fig. 12. C_d versus Re.

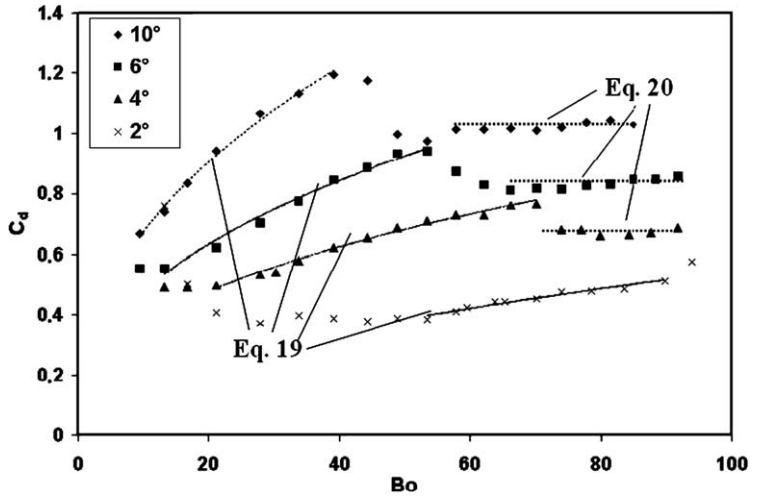

Fig. 13. C_d versus Bo. Eq. (19) is plotted for the inclination angles of 2°, 4°, 6° and 10° while Eq. (20) is plotted for 4°, 6° and 10° of inclination.

regions (principally at low angles) and for the transition between two sub-regimes, the reader is referred to Figs. 12 or 13. The drag coefficient in the *deformable bubble* sub-regime is given by

$$C_d = A(\theta)Bo^{0.450} \tag{17}$$

where A is

$$A(\theta) = 0.040\theta^{0.773} \tag{18}$$

Therefore, the drag coefficient is expressed by

$$C_d = 0.040\theta^{0.773}Bo^{0.450} \tag{19}$$

In the *bulged bubble* sub-regime, the drag coefficient is approximated by

$$C_d = 0.354\theta^{0.473} \tag{20}$$

In both expressions, the inclination angle is given in degrees. The correlations 19 and 20 include all the experimental data with a maximal deviation of 5%. The range of validity for these equations is given in Table 2. At high inclination angles almost all the values of C_d in the studied range of Bo may be given by Eqs. (19) and

Table 2
Limits of the *deformable* and *bulged* sub-regimes

Inclination (°)	Deformable bubble	Bulged bubble
2	$53 \leqslant Bo \leqslant 90$	–
3	$33 \leqslant Bo \leqslant 87$	–
4	$21 \leqslant Bo \leqslant 70$	$73 \leqslant Bo \leqslant 92$
6	$13 \leqslant Bo \leqslant 53$	$57 \leqslant Bo \leqslant 92$
8	$13 \leqslant Bo \leqslant 44$	$53 \leqslant Bo \leqslant 92$
10	$9 \leqslant Bo \leqslant 40$	$48 \leqslant Bo \leqslant 85$

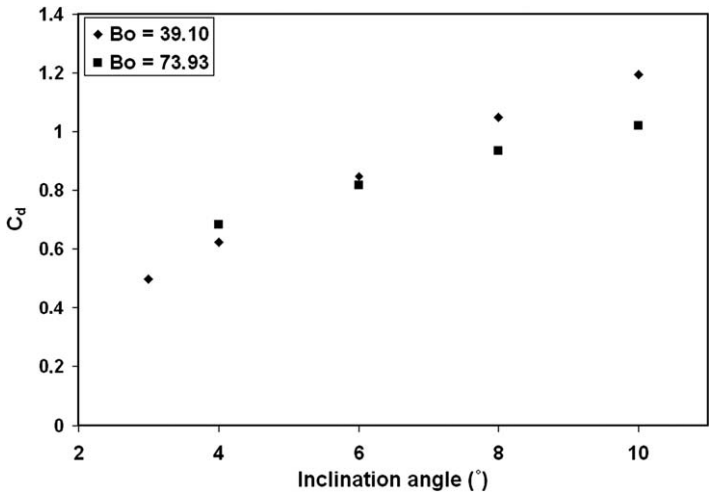

Fig. 14. C_d versus inclination angle for two different bubble sub-regimes.

(20). As we have already mentioned, the transition between sub-regimes is not sharp. Consequently, the values of the Bond number at the onset of the different sub-regimes as presented in Table 2 are only estimates. Fig. 14 shows the variation of the drag coefficient as function of the inclination angle for two different bubble sub-regimes. The values of $Bo = 39.10$ and 73.93 correspond to the *deformable* and to the *bulged bubble* sub-regimes, respectively. The rate of increase of the drag coefficient with the inclination angle is larger for the *deformable bubble* and rather linear for both sub-regimes.

To resume, expressions (Eqs. (19) and (20)) for the drag coefficient in the *deformable* and *bulged bubble* sub-regimes have been given. At high inclination angles, the equations cover almost all the values of the drag coefficient in the range of Bond number studied in this work.

4. Conclusions

In this work, the influence of bubble volume and inclination angle on the terminal velocity of a moving bubble under a surface has been studied in details. Distilled water and air were used in the two-phase gravity driven system. The solid surface was represented by a plate of plexiglas. A track-mounted high-speed camera was used to capture the characteristics of the moving bubble. The angles of inclination were varied from 2° to 10°. The Bond number covered the range from about 10 to 100. In the studied ranges, the results have shown that

- In the wetting regime, studied in this work, the increase of the terminal velocity with the bubble volume is not monotonous at a given inclination. Indeed, four sub-regimes, each corresponding to a characteristic bubble shape have been found.

- The terminal velocity increases with the inclination angle at a given bubble volume. The increase is very important for both low bubble volumes and low inclination angles. For high bubble volumes the increase is more linear.
- The inertia controls principally the terminal velocity of the *bulged bubbles*. Surface tension and viscous forces play a role for bubbles at low angles and small bubble volumes.
- The values of the drag coefficient have been evaluated. The shape of the curves has similarities with those for the classical vertical rising bubble. Expressions of the form $C_d = C_d(Bo, \theta)$ in the *deformable* (Eq. (19)) and $C_d = C_d(\theta)$ in the *bulged bubble* (Eq. (20)) sub-regimes.

In a next step, the influence of the material properties of the working liquid on the motion of single bubbles will be studied. A fiber optic sensor has also been developed in order to measure the thickness of the wetting film. The analysis of the results is ongoing.

Acknowledgements

The first author gratefully acknowledges the support of the Fonds québécois de recherches sur la nature et les technologies (FQRNT) and that of the Conseil de Recherches en Sciences Naturelles et en Génie du Canada (CRSNG) in the form of post-graduate scholarships. The authors also thank to Mr. Sylvain Desgagné for the technical assistance.

References

Bertherton, F.P., 1961. The motion of long bubbles in tubes. J. Fluid Mech. 10, 166–188.
Chen, J. J. J., Jianchao, Z., Kangxing, Q., Welch, B. J., Taylor, M. P., 1992. Rise velocity of air bubbles under a slightly inclined planed submerged in water, The Fifth Asian Congress of Fluid Mechanics, pp. 1173–1176.
Cheung, F.B., Haddad, K.H., 1997. A hydrodynamic critical heat flux model for saturated pool boiling on a downward facing curved heating surface. Int. J. Heat Mass Transfer 40, 1291–1302.
Clift, R., Grace, J.R., Weber, M.E., 1978. Bubbles, Drops, and Particles. Academic Press, New York, 380 pp.
Davies, R.M., Taylor, S.G., 1950. The mechanics of large bubbles rising through extended liquids and through liquids in tubes. Proc. R. Soc. Ser. A 200, 375–390.
Ellingsen, K., Risso, F., 2001. On the rise of an ellipsoidal bubble in water: oscillatory paths and liquid-induced velocity. J. Fluid Mech. 440, 235–268.
Fortin, S., Gerhardt, M., Gesing, A. J., 1984. Physical modelling of bubble behaviour and gas release from aluminum reduction cell anodes, TMS Light Metals, pp. 721–741.
Goldsmith, H.L., Mason, S.G., 1962. The movement of single large bubbles in closed vertical tubes. J. Fluid Mech. 14, 42–58.
Haberman, W.L., Morton, R.K., 1953. Davis Taylor Model Basin, NR 715-102.
Hartland, S., Hartley, R.W., 1976. Axisymmetric Fluid–Liquid Interfaces. Elsevier Scientific Publishing Company, 782 pp.
Hartunian, R.A., Sears, W.R., 1957. On the instability of small bubbles moving uniformly in various liquid. J. Fluid Mech. 3, 27–47.
Haupin, A., 1971. Scanning reference electrode for voltage contours in aluminum smelting cells. J. Met. 23, 46–49.
Kiss, L.I., Poncsák, S., Toulouse, D., Perron, A., Liedtke, A., Mackowiak, V., 2004. Detachment of bubbles from their nucleation sites, TMS Light Metals, Multiphase Phenomena and CFD Modeling and Simulation in Materials Processes, pp. 159–167
Masliyah, J., Jauhari, R., Gray, M., 1994. Drag coefficients for air bubbles rising along an inclined surface. Chem. Eng. Sci. 49, 1905–1911.
Maxworthy, T., 1991. Bubble rise under an inclined plate. J. Fluid Mech. 229, 659–674.
Maxworthy, T., Gnann, C., Kürten, M., Durst, F., 1996. Experiments on the rise of air bubbles in clean viscous liquids. J. Fluid Mech. 321, 421–441.
Mendelson, H.D., 1967. The prediction of bubble terminal velocities from wave theory. AIChE J. 13, 250–253.
Peebles, F.N., Garber, H.J., 1953. Studies on the motion of gas bubble in liquid. Chem. Eng. Prog. 49, 88–97.
Perron, A., Kiss, L. I., Poncsák S., 2005. Regimes of the movement of bubbles under the anode in an aluminum electrolysis cell, TMS Light Metals, pp. 565–570.
Pruppacher, H.R., Klett, J.D., 1978. Microphysics of clouds and precipitation. D. Reidel, Boston, 714 pp.
Saffman, P.G., 1956. On the rise of small air bubbles in water. J. Fluid Mech. 1, 249–275.
Solheim, A., Thonstad, J., 1986. Model cell studies of gas induced resistance in Hall–Heroult cells. Light Metals, 397–403.
Spedding, P.L., Nguyen, V.T., 1978. Bubble rise and liquid content in horizontal and inclined tubes. Chem. Eng. Sci. 33, 987–994.
Tomiyama, A., Kataoka, I., Zun, I., Sakaguchi, T., 1998. Drag coefficients of single bubbles under normal and micro gravity conditions. JSME Int. J. Ser. B 41, 472–479.
Tomiyama, A., Celata, G.P., Hosokawa, S., Yoshida, S., 2002. Terminal velocity of single bubbles in surface tension force dominant regime. Int. J. Multiphase Flow 28, 1497–1519.

White, F.M., 1999. Fluid Mechanics, fourth ed. McGraw-Hill, 826 pp.
Zoric, J., Solheim, A., 2000. On gas bubbles in industrial aluminum cells with prebaked anodes and their influence on the current distribution. J. Appl. Electrochem. 30, 787–794.
Zukoski, E.E., 1966. Influence of viscosity, surface tension and inclination angle on motion of long bubbles in closed tubes. J. Fluid Mech. 25, 821–837.